D 2 Spin-ice materials and magnetic monopoles

Thomas Lorenz
Physics Institute II
University of Cologne

Contents

Lecture Notes of the 48^{th} IFF Spring School "Topological Matter – Topological Insulators, Skyrmions and Majoranas" (Forschungszentrum Jülich, 2017).

1 Introduction

Spin ice describes a class of magnetic systems where competing microscopic interactions and geometric constraints prevent the formation of ordinary long-range magnetic order. It was discovered about 20 years ago by the observation [1] that the low-temperature magnetic state of $Ho_2Ti_2O_7$ realizes a magnetic analogue of ordinary water ice. Both ices have in common that their classical groundstate hosts a finite residual entropy, which results from the so-called Bernal-Fowler ice rules [2] and has been explained by Pauling [3] back in the 1930s. From neutron scattering experiments [4, 5] it is inferred that the zero-field, low-temperature magnetic state is highly correlated, but there is no long-range magnetic order, which would be identified by well-defined magnetic Bragg peaks. In this respect, spin ice strongly resembles so-called spin liquids [6]. Spin liquids very often also arise from magnetic frustration, but in most cases there is, in addition, a reduced dimensionality, which prevents the formation of long-range magnetic order. Spin-liquid materials cover an extremely wide field ranging from, e.g., the one-dimensional antiferromagnetic spin-1/2 Heisenberg chain, whose groundstate was solved by Bethe already in 1931 [7], to the high-T_c cuprate superconductors, which arise from charge-carrier doped two-dimensional spin liquids. In contrast to spin-liquid materials, the number of spin-ice materials is rather limited and they usually arise from the three-dimensional pyrochlore structure. Spin ice can be realized in some other structures, too, and there is also two-dimensional, so-called artificial spin ice [8, 9], but I will concentrate on the two prototype spin-ice materials $Ho_2Ti_2O_7$ and $Dy_2Ti_2O_7$. Another similarity of spin ice and spin liquids concerns their elementary excitations, which in both cases may consist of so-called pairs of fractionalized particles. For spin ice, it has been predicted that, instead of ordinary magnetic dipolar excitations, the magnetic excitation spectrum rather resembles that of pairs of more or less unbound magnetic monopoles [10, 11]. These predictions triggered a lot of experimental investigations that tried to identify clear signatures of magnetic monopole charges. The following sections will give an overview of the basic concepts and models to describe spin-ice physics, some fundamental experimental data supporting these models will be presented, and I will also touch various open questions, which require further studies.

2 Magnetic frustration and the pyrochlore structure

Because one basic ingredient of spin-ice physics is a geometric frustration of the magnetic interactions, we will first consider some simple examples of magnetic frustation. In Fig. 1(a), we assume a triangular arrangement of Ising spins with collinear easy axes and antiferromagnetic interactions. Whenever 2 spins are oriented antiparallel to each other, the 3^{rd} one is frustrated, because both possible orientations can satisfy only 1 of the 2 remaining bonds. Note that the restriction to Ising spins is important here, because for Heisenberg spins an 120° orientation of all 3 spins will minimize the total energy. It is also obvious, that there is no magnetic frustration if the interaction is ferromagnetic and all 3 spins can point parallel to each other. This situation changes, however, if we are dealing with Ising spins with non-collinear easy axes connecting the center of the triangle with the respective corners, as is sketched in Fig. 1(b). In this case, each spin pointing inwards would favor the other 2 pointing outwards, and vice versa, but, as in (a), only 2 bonds can be satisfied while the 3^{rd} bond remains unsatisfied. In Fig. 1(c), the triangle is extended to a tetrahedron such that we are now dealing with a 3-dimensional arrangement of 4 Ising spins with non-collinear easy axes from each corner to the center of the tetrahedron. Be-

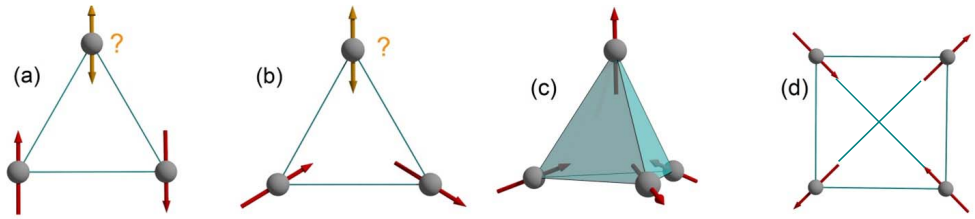

Fig. 1: *Ising spins with geometric frustration.*

cause each spin may either point into or out of the tetrahedron, there are $2^4 = 16$ possible spin configurations: "4in", "4out", 4 × "3in-1out", 4 × "1in-3out", and 6 × "2in-2out". The energetic order of these configurations can be easily obtained by balancing satisfied with unsatisfied bonds and, for convenience, one may use the mapping of the 3-dimensional tetrahedron to a 2-dimensional square with 6 equivalent bonds, see Fig. 1(d). Because ferromagnetic intercation favors in-out spin orientations, 4in and 4out result in 6 unsatisfied bonds, for 3in-1out as well as for 1in-3out 3 satisfied cancel with 3 unsatisfied bonds, while the 2in-2out configurations have 4 satisfied and only 2 unsatisfied bonds. Thus, the groundstate is given by the 2in-2out configurations and remains sixfold degenerate. Of course, this consideration is oversimplified, because a single tetrahedron is considered within a classical picture, but it will be seen that this model already yields a good basis to understand many properties of the most studied spin-ice materials $Ho_2Ti_2O_7$ and $Dy_2Ti_2O_7$. These materials and also the corresponding, and partially very complex, theoretical models describing them are often referred to as "classical spin-ice materials/models" in order to emphasize that quantum effects are so small that they are usually completely ignored [12]. This is different for so-called "quantum spin-ice materials/models" where the description based on pure Ising moments is no longer applicable [13, 14]. The latter will not be discussed within this lecture.

The spin-ice materials crystallize in the so-called pyrochlore structure with a large, cubic unit cell with lattice parameter $a \approx 10$ Å containing 8 formula units. In order to understand the magnetism, we concentrate on the magnetic rare-earth ions R^{3+} and their local evironments. As displayed in Fig. 2, the R^{3+} ions form a network of corner-sharing tetrahedra, whose edges point along the 6 equivalent $\{110\}$ directions of the cubic structure and each triangular face is perpendicular to one of the 4 equivalent $\{111\}$ diagonals. The partially filled $4f$-shell occupation is dominated by the centrosymmetric nuclear potential such that the free-ion Hund's rules are applicable. Thus, the $4f$ quantum numbers for Dy^{3+} (Ho^{3+}) are $S = 5/2$ (2), $L = 5$ (6), and $J = 15/2$ (8) with g-factors $g_J = 4/3$ (5/4). The $(2J + 1)$-fold degeneracy of this (atomic) groundstate term is then lifted by the crystal electric field from the surrounding ions and it turns out that for both, Dy^{3+} and Ho^{3+}, the lowest-lying orbital is a doublet-state $|GS\rangle \simeq |\pm J_z^{max}\rangle$ with local $\{111\}$ quantization axes. Contributions from other J_z quantum numbers to $|GS\rangle$ are in the %-range only and the crystal electric field is so strong that it results in an energy difference $\Delta E/k_B > 200$ K to the first excited state.[1] Thus, for the low-temperature magnetism it is sufficient to consider local magnetic moments $\mu \simeq g_J \mu J_z^{max} = 10\mu_B$ which may point either into or out of the tetrahedra. This exactly realizes the Ising spins with non-collinear easy axes of the model in Fig. 1(c).

Concerning the magnetic interactions, there are 2 important aspects to consider: (i) the inner $4f$ orbitals have little overlap with those of the neighboring ions, such that exchange interaction

[1] From now on, energies will be given in K without the explicite Boltzmann factor k_B in the denominator.

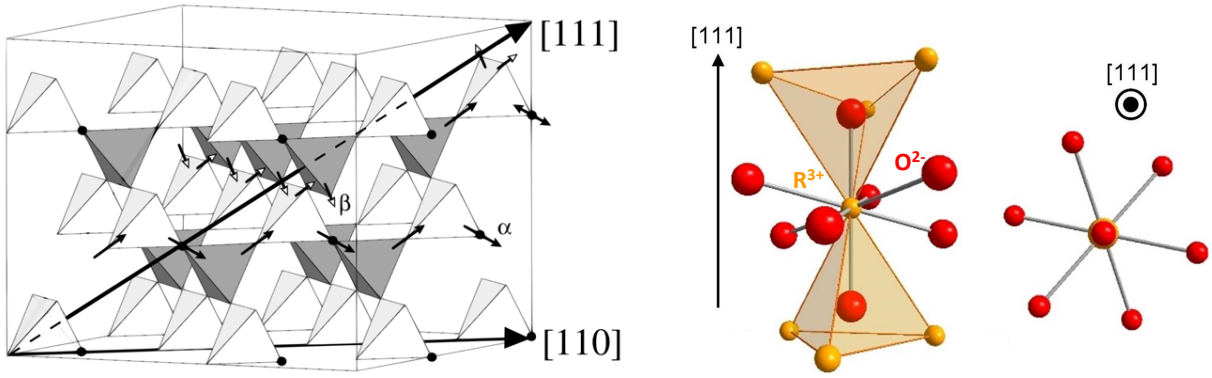

Fig. 2: *Left: The cubic pyrochlore structure contains a network of corner-sharing tetrahedra of magnetic rare-earth ions R^{3+}. This can be also viewed as sets of α and β chains running along $[110]$ and $[1\bar{1}0]$, respectively. Right: Each R^{3+} ion is surrounded by 8 nearest neighbor O^{2-} ions forming slightly distorted cubes with trigonal symmetry around the local [111] axes.*

energies J_{ex} are weak, and (ii) the large magnetic moments $\mu \simeq 10\,\mu_{\mathrm{B}}$ result in a comparatively large dipole-dipole energy $D_{nn} \simeq 2.35$ K for a nearest-neighbor distance $r_{nn} \simeq 3.54$ Å. Following the notation of [15], the corresponding hamiltonian is

$$\mathcal{H} = -J_{ex} \sum_{\langle (i,a),(j,b) \rangle} \vec{S}_i^a \cdot \vec{S}_j^b + \frac{\mu_0 \mu^2}{4\pi} \sum_{\substack{i>j \\ a,b}} \frac{\vec{S}_i^a \cdot \vec{S}_j^b}{|\vec{R}_{ij}^{ab}|^3} - \frac{3(\vec{S}_i^a \cdot \vec{R}_{ij}^{ab})(\vec{S}_i^b \cdot \vec{R}_{ij}^{ab})}{|\vec{R}_{ij}^{ab}|^5} \,. \tag{1}$$

Here, the vectors $\vec{S}_i^a = \sigma_i^a \hat{z}^a$ denote Ising spins with normalized local easy axes $\hat{z}^a$ along the different $\{111\}$ directions, $\sigma_i^a = \pm 1$ according to the two possible spin orientations and the vectors $\vec{R}_{ij}^{ab}$ connect the lattice sites of $\vec{S}_i^a$ and $\vec{S}_j^b$. Note that the long-range character of the dipolar interaction makes Eq. (1) very complex. As an approximation, we restrict to the nearest-neighbor dipolar interactions, which favor a ferromagnetic alignment of the magnetic moments as displayed in Fig. 1(c). Thus, Eq. (1) simplifies to an effective nearest-neighbor hamiltonian

$$\mathcal{H} = -3\, J_{eff} \sum_{\langle (i,a),(j,b) \rangle} \vec{S}_i^a \cdot \vec{S}_j^b - \mu \sum_i \vec{S}_i \cdot \vec{B} \,. \tag{2}$$

Here, $J_{eff} = J_{ex} + D_{nn}$ and the additional second addend considers the Zeeman energy in the presence of an external magnetic field[2]. The comparison between this so-called single-tetrahedron approximation (2) and the experimental results of $Dy_2Ti_2O_7$ and $Ho_2Ti_2O_7$ reveal $J_{eff} \simeq 1.1$ K and $\simeq 1.8$ K, respectively [16, 17]. Thus, for both materials the bare exchange interaction J_{ex} is antiferromagnetic and actually competes with the dipolar interaction D_{nn}. In other words, D_{nn} is the driving force of the spin-ice behavior in these materials, which are therefore also referred to as dipolar spin ices.

3 Spin ice in a magnetic field

Figure 3 displays the energy levels of $Dy_2Ti_2O_7$ and $Ho_2Ti_2O_7$ according to the single tetrahedron approximation. It is easy to see that each of the 2in-2out configurations results in a

[2]The factor of 3 compensates $\hat{z}^a \hat{z}^b = -1/3$ due to the non-collinear easy axes.

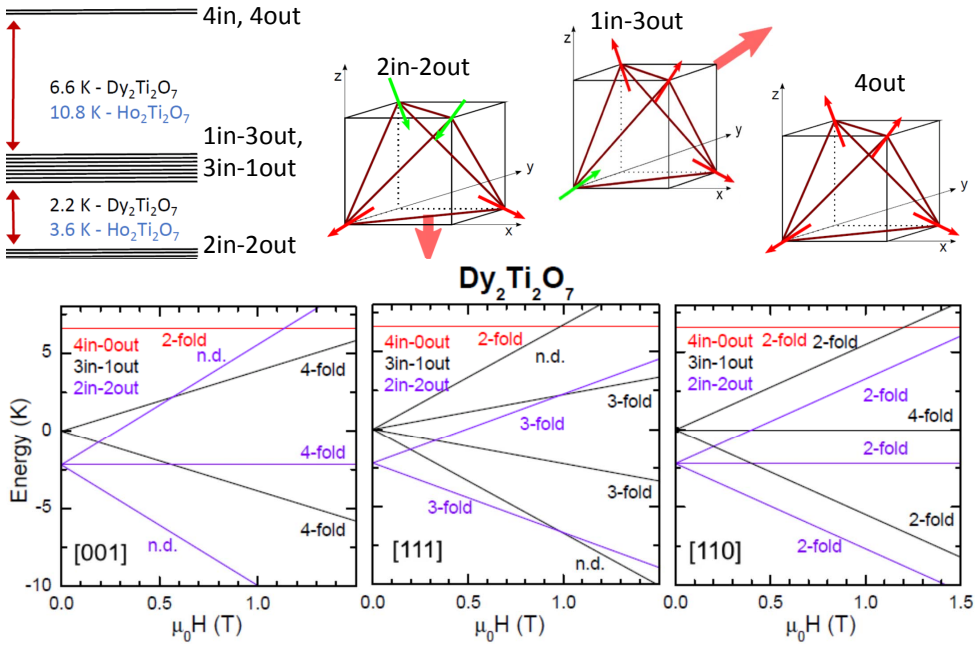

Fig. 3: *Top: Energy levels of dipolar spin ices. The "2in-2out" configurations carry a net magnetic moment pointing along one of the* $\pm\{100\}$ *cubic axes reflecting the sixfold degeneracy. The eightfold degenerate "3in-1out" or "1in-3out" states have moments along one of the* $\pm\{111\}$ *diagonals, while "4in" and "4out" are nonmagnetic. Bottom: Zeeman splitting of the energy levels of* $Dy_2Ti_2O_7$ *for magnetic fields applied along* $[001]$, $[111]$, *and* $[110]$.

magnetic moment of $10/\sqrt{3}\,\mu_B \simeq 5.77\,\mu_B$ per ion, which points along one of the $\pm\{100\}$ cubic axes reflecting the sixfold degeneracy. The eightfold degenerate 3in-1out/1in-3out states yield $5\,\mu_B$ per ion pointing along one of the $\pm\{111\}$ diagonals. Finally, the 4in and 4out states are nonmagnetic because the individual moments fully compensate each other. External magnetic fields cause a Zeeman splitting of the energy levels with finite magnetic moments and the lifting of these degeneracies depends on the magnetic-field direction. A field parallel to one of the cubic axes immediately lifts the groundstate degeneracy completely, because it splits off the 2in-2out configuration whose magnetization is parallel to the field. The energy of the state with the opposite magnetization increases, while the other four states with magnetizations perpendicular to the field remain unchanged. In addition, the 3in-1out/1in-3out levels split into 2 sets of fourfold degenerate states.

Fields along one of the diagonals $\{111\}$ first reduce the groundstate degeneracy from six-to threefold until a critical H_c is reached, where a level crossing to a non-degenerate groundstate occurs. This high-field groundstate has one moment parallel to the field and three moments with finite components along the field direction. As shown in Fig. 2, the pyrochlore structure consists of planes of tetrahedra of alternating orientations stacked along the $\{111\}$ directions. Thus, the high-field groundstate for H along one of these diagonals is given by alternating planes of 3in-1out and 1in-3out states stacked along the field direction. The threefold degenerate groundstate for $0 < H < H_c$ is called Kagome-ice state. It consists of an alternating stacking of triangular planes formed by the fully polarized moments at the tips of the tetrahedra and Kagome planes which arise from the corresponding bottom triangles of tetrahedra; see Fig. 2. On each of theses triangles, only 2 moments have a finite component along the field, while the third has a finite component in the opposite direction in order to fulfill the 2in-2out ice rule. The Kagome-ice

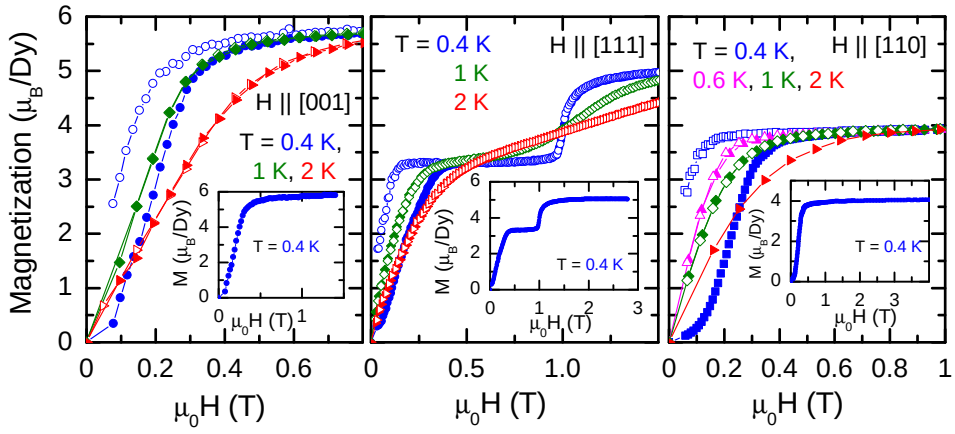

Fig. 4: *Magnetization of $Dy_2Ti_2O_7$ for different field directions obtained with increasing (•) and decreasing (○) field. The insets show the lowest-temperature data up to larger fields.*

state is stable up to $\mu_0 H_c \simeq 1$ T in $Dy_2Ti_2O_7$ and up to $\simeq 1.6$ T in $Ho_2Ti_2O_7$ and this difference directly reflects the different zero-field splittings of the corresponding energy levels.

For magnetic fields applied along one of the $\{110\}$ directions the magnetic structure of spin ice is best described by so-called α chains and β chains. This is due to the fact that each tetrahedron has 2 moments which align with a finite component along the field direction such that one of them points into and the other out the tetrahedron. As can be seen from Fig. 2, these spins form chains of ferromagnetically aligned Ising spins of alternating easy-axis orientations, which are called α chains and are running parallel to the field. The remaining 2 spins of the tetrahedra also form chains, which are oriented perpendicular to the field. The corresponding easy-axis direction along these β chains also alternates, but it remains within the plane perpendicular to the field and, thus, the magnetic field does not affect the spin orientation. Because of the ferromagnetically aligned α spins, the β spins also align ferromagnetically with respect to each other, in order to fulfill the 2in-2out ice rule, and for a single tetrahedron there remains a twofold right-left degeneracy, see Fig. 3. Because in the pyrochlore structure the β spins are connected, they also form ferromagnetically aligned β chains and therefore this twofold degeneracy vanishes with increasing chain length. As a consequence, the β chains (induced by the transverse field along the α chains) resemble ordinary ferromagnetic Ising chains in zero magnetic field.

Figure 4 displays characteristic low-temperature magnetization curves of $Dy_2Ti_2O_7$ measured for magnetic fields applied along the different high-symmetry directions. For $H\|[001]$ the magnetization rapidly approaches saturation of about $5.8\,\mu_B$/Dy, which is very close to the expected value of $5.77\,\mu_B$/Dy when all tetrahedra are in the 2in-2out configuration with the net moment along the field direction. For $H\|[111]$, the high-field saturation of about $5\,\mu_B$/Dy also agrees very well with the expected value for an alternating stacking of planes with 3in-out and 1in-3out tetrahedra. Moreover, below 1 K the magnetization develops a plateau at $3.3\,\mu_B$/Dy as expected for the above-described Kagome-ice state. The width of this plateau increases on decreasing temperature and the level-crossing transition at a critical field of $\mu_0 H_c \simeq 1$ T systematically sharpens. Finally, the magnetization curves for $H\|[110]$ are of similar shape as those for $H\|[001]$, but saturate at a smaller value of about $4\,\mu_B$/Dy, which again agrees well to the value of $4.08\,\mu_B$/Dy expected for fully polarized α chains and β chains, which do not contribute. For all three field directions, pronounced hysteresis effects develop at the lowest temperatures and there is a remnant magnetization when the field is decreased back to zero. It

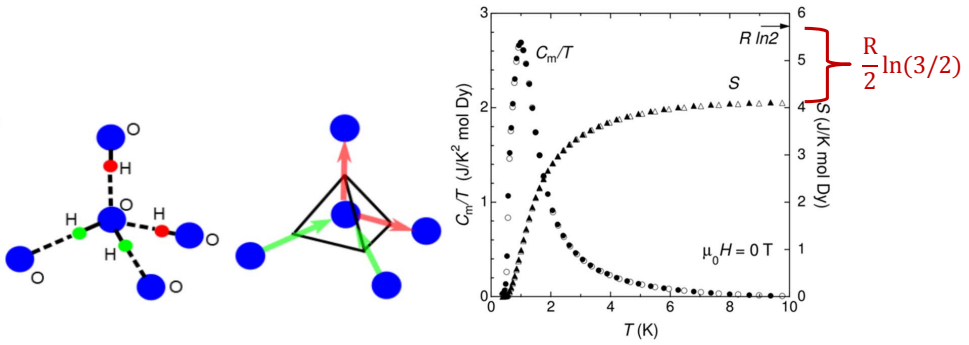

Fig. 5: *Left: 2in-2out hydrogen arrangement in hexagonal water ice compared to the analogous spin orientations in spin ice. Right: Magnetic specific heat C_m/T and the corresponding magnetic entropy S of $Dy_2Ti_2O_7$ [18] (closed symbols) together with Monte Carlo simulations (open symbols) of the dipolar spin-ice model. (extracted from [4]).*

is also found (but not shown here) that the remnant magnetization slowly decreases as a function of time and the hysteresis width depends on the field sweep rate. All these observations reveal that the spin ice only very slowly reaches thermal equilibrium at low temperature. Apart from this slow thermal equilibration, the principle behavior of the magnetization can be well understood within the single-tetrahedron approximation.

4 Water ice and residual entropy

The solid phases of water ice form a very complex field of research and, depending on the external parameters, about 20 different phases of crystalline or amorphous forms of solid ice are reported; for a review see [19]. In the context of spin ice, we can restrict to the most common form of solid water ice, so-called hexagonal ice Ih, which forms when water freezes under ambient conditions. The term "spin ice" is used to express the close analogy between the alignments of the Ising moments and the hydrogen (or almost the H^+ proton) arrangement in hexagonal water ice. There, each O atom is tetrahedrally coordinated by 4 neighboring O atoms and each of the 4 bonds is occupied by 1 H atom. This is the first of the so-called Bernal-Fowler ice rules formulated back in 1933 [2]. The second one is the 2in-2out ice rule, which states that 2 H atoms of the 4 bonds are closer to the O atom and the other 2 H atoms are further away, and follows from the fact that water ice consists of H_2O molecules. As is shown Fig. 5, the 6 different possibilities of arranging the H atoms in each tetrahedron exactly corresponds to the possible alignments of the Ising magnetic moments in spin ice. Also in the 1930s, it was found experimentally via heat capacity measurements [20, 21] that hexagonal water ice has a finite residual entropy, which was explained by Pauling to result from the randomness of the proton arrangement [3]. The so-called Pauling approximation considers that water ice of N molecules has in total 2^{2N} possibilities to arrange the H atoms, but only the fraction $(6/16)^N$ of them fulfills the 2in-2out rule. This then results in Pauling's molar residual entropy[3]

$$S_{\mathrm{P}} = \frac{1}{2} k_{\mathrm{B}} \ln\left(\frac{3}{2}\right)^{N_{\mathrm{A}}} = \frac{N_{\mathrm{A}} k_{\mathrm{B}}}{2} \ln\left(\frac{3}{2}\right) = \frac{R}{2} \ln\left(\frac{3}{2}\right) \simeq 1.69 \ \frac{\mathrm{J}}{\mathrm{mol\ K}} \ . \tag{3}$$

[3]The additional prefactor $1/2$ arises because the position of each H atom is related with 2 neighboring O atoms.

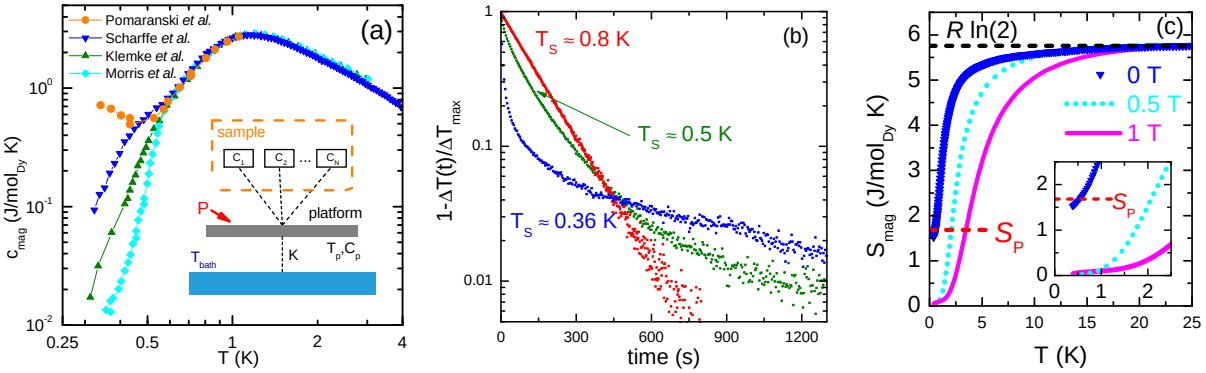

Fig. 6: *(a) Low-temperature specific heat of $Dy_2Ti_2O_7$ from [22, 23, 24, 5]. The inset sketches a sample containing different (e.g. phononic, magnetic, ...) subsystems, which may be out of thermal equilibrium, if their thermal coupling is weak. This results in highly non-exponential time dependences $\Delta T(t) = T_{\rm P}(t) - T_{\rm bath}$ between the platform and bath temperatures as is observed in [22, 23, 24] and is shown in (b) for (average) sample temperatures $T_{\rm S} < 0.8$ K [23]. (c) Magnetic entropy change obtained in [23] for $Dy_2Ti_2O_7$ in magnetic fields $\mu_0 H = 0$, 0.5, and 1 T applied along [001]. $S_{\rm mag}(25\ {\rm K}, H)$ is adjusted to the full magnetic entropy $R\ln(2)$ (black dashed line) and Pauling's residual entropy from Eq. (3) is shown by the red dashed line.*

Concerning the spin-ice materials, the magnetic contribution to the specific heat has been analyzed and, in fact, for $Dy_2Ti_2O_7$ the entropy change from about 0.2 to 15 K has been found [18] to differ from the full entropy $R\ln(2)$ by almost exactly the value of $S_{\rm P}$. Moreover, it has been also shown [4] that the experimental data over the entire temperature range are well reproduced by Monte Carlo simulations of the dipolar spin-ice model; see Fig. 5. A natural question in this context arises from the conflict of the finite residual groundstate entropy of the dipolar spin-ice model with the 3^{rd} law of thermodynamics (Nernst's theorem) predicting a vanishing entropy at zero temperature. Thus, there were a lot of efforts to clarify whether some kind of magnetic order finally evolves at low-enough temperature, but until now no such order could be proven experimentally. Of course, one may always argue that the experimentally obtained temperatures were not yet low enough, but independent from this principle problem, there are other issues which complicate the situation in the dipolar spin-ice materials. For $Ho_2Ti_2O_7$, a large specific-heat contribution from the nuclear moments completely dominates the measured low-temperature specific-heat data and prevents an unambiguous separation of the low-temperature magnetic entropy [8].

For $Dy_2Ti_2O_7$, the main problem arises from the above-mentioned problem of slow thermal equilibration, which makes measurements of the low-temperature specific heat very problematic. This has been pointed out independently by different groups [22, 23, 24] during the last years and, as shown in Fig. 6(a), the published low-temperature c_p data of $Dy_2Ti_2O_7$ differ by up to almost 2 orders of magnitude. Standard techniques to measure c_p typically use rather short (usually less than a few minutes) heat pulses and result in small c_p values [5, 18], whereas significantly larger c_p values are obtained when for each data point thermal equilibration times of the order of 10–20 minutes are used [23, 24, 25]. As pointed out, however, in [22] thermal equilibration times of up to many hours may become relevant at lowest temperature and according to this report $c_p(T)$ re-increases below about 0.4 K. Phenomenologically, this behavior can be described by assuming that a sample consists of different, e.g. one (or several) phononic, nuclear, or magnetic, subsystems with individual heat capacities C_i and thermal couplings k_{ij}

between them, as sketched in Fig. 6(a). As long as these couplings are large, any heat transferred to the sample is distributed over all subsystems proportional to the magnitudes of the C_i and defines a common sample temperature T_S. With respect to the experimental determination of the specific heat, this means: if all internal k_{ij}'s (and the coupling of at least one of them to the sample platform) are much larger than the thermal coupling K between platform and an external heat bath, T_S will be equal to the measured platform temperature T_P and any temperature difference $\Delta T(t) = T_{\rm P}(t) - T_{\rm bath}$ will evolve exponentially as a function of time t with a single relaxation time $\tau = C/K$ where $C = \sum_i C_i$. As is shown in Fig. 6(b), this is well fulfilled for $Dy_2Ti_2O_7$ at $T_S \simeq 0.8$ K, where the semilogarithmic plot of $1 - \Delta T(t)/\Delta T_{\rm max}$ is a straight line. However, a strong curvature develops on decreasing temperature and the resulting c_p values sensitively depend on the methods used for its extraction. Of particular importance is the time window, over which $\Delta T(t)$ is measured, and the width of the experimentally accessible window depends on the experimental setup. An increasing time window allows for a better thermalization of the sample, but it also requires an extreme stability of all experimental parameters over such long time, because for non-exponential $\Delta T(t)$ curves c_p is obtained by time integration of $\Delta T(t)$. Thus, an unambiguous determination of c_p down to the lowest temperature remains problematic.

What does this ambiguity mean in the context of Pauling's residual entropy? Because the various experimental data sets agree well above about 0.5 K, we will first concentrate on this higher temperature range. Because experimentally only entropy changes can be determined, one has to fix the magnetic entropy at some point, e.g. to $R\ln(2)$ at high-enough temperature. For $Dy_2Ti_2O_7$, $T \approx 25$ K should be sufficient, because all energy levels are below 10 K (see Fig. 3). In addition, an estimate of the phononic background is required, which can be obtained from measurements of nonmagnetic reference materials, e.g. $Y_2Ti_2O_7$ [23], and this estimate can be checked by considering the total entropy change in a finite magnetic field, which causes a non-degenerate ground state. As shown in Fig. 6(c), the resulting entropy change in external fields of 0.5 or 1 T $\|[001]$ agrees very well with the expected $R\ln(2)$. In contrast, the zero-field entropy for $T \simeq 0.5$ K is very close to Pauling's residual entropy $S_{\rm P}$. The slightly different absolute values of $S_{\rm P}$ and the experimental result should not be overinterpreted. However, there is a significant slope $\partial S/\partial T = c_{\rm mag}/T$ in the experimental data and according to Pomaranski *et al.* [22] this slope considerably increases with further decreasing temperature. This approximate plateau-like feature of the entropy is one justification that down to $T \simeq 0.5$ K $Dy_2Ti_2O_7$ approaches the degenerate ground state of the classical dipolar spin ice. However, with further decreasing temperature some kind of ordered ground state seems to evolve ultimately. One may expect this to occur due to quantum effects, additional weaker interactions, and/or magnetoelastic coupling, but the real groundstates of this and other (quantum) spin-ice candidates are in most cases not known, see e.g. [12, 14, 26]. Recently, various ordered groundstates for $Dy_2Ti_2O_7$ have been suggested, which can arise depending on the strength of quantum tunneling [27]. Moreover, weak non-magnetic dilution may induce transitions to a so-called topological spin glass [28].

5 Magnetic monopole excitations

Up to this point, mainly the unusual ground state of dipolar spin ice has been discussed, but even more exotic are the low-lying excitations. Although these excitations result from magnetic dipole excitations, it turns out that the dipole excitations can fractionalize into pairs of

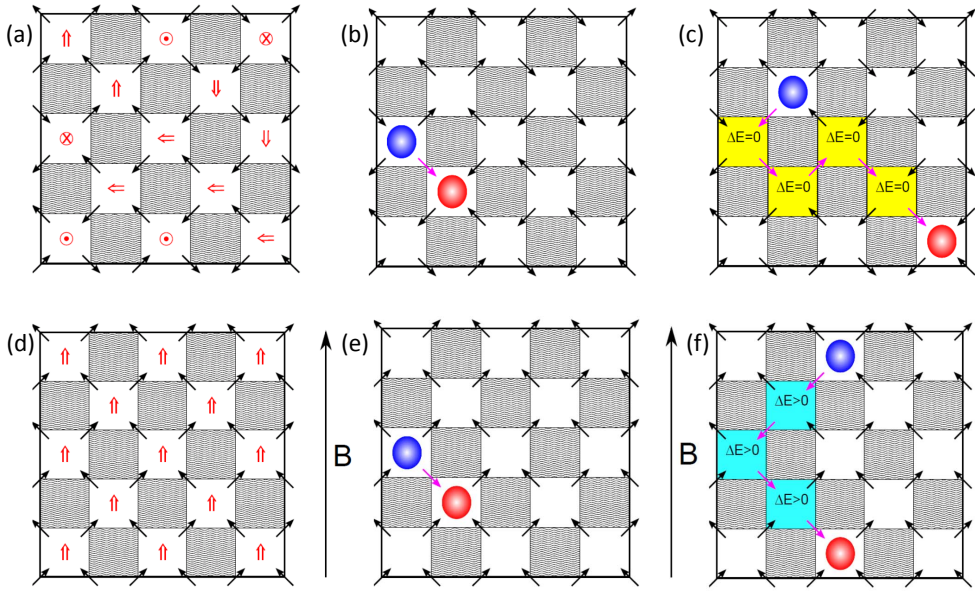

Fig. 7: *Fractionalization of magnetic dipoles to monopole-antimonopole pairs. White squares represent tetrahedra with 4 Ising moments (black arrows); each of them belongs to 2 neighboring tetrahedra. (a) In zero field, each square is in one of the sixfold 2in-2out states. Red arrows represent the corresponding net moments, pointing along one of the six cubic* $\{001\}$ *directions. (b) A single spin flip excites neighboring 3in-1out/1in-3out states, which can move independently over the lattice via single flips without additional energy cost, because the marked arrows of the yellow squares in (c) switched between degenerate 2in-2out states. (d) A magnetic field along* $[001]$ *fixes a particular 2in-2out configuration as the groundstate, (e) a neighboring pair of 3in-1out/1in-3out excitations needs additional Zeeman energy, and (f) each step of separating them induces additional Zeeman-excited 2in-2out states marked by blue squares.*

magnetic monopoles and anti-monopoles (north and south poles) that, for zero magnetic field, may propagate almost independently over the lattice. The basic idea for this fractionalization is sketched in Fig. 7, where for simplicity the 3-dimensional pyrochlore lattice is mapped to 2 dimensions [4]. As in Fig. 1(c,d), each tetrahedron is expressed by a square and the corner-sharing pyrochlore structure then transforms to a checkerboard, where one type of squares, e.g. the white ones, represent the tetrahedra. In zero field, each tetrahedron chooses one of the sixfold degenerate 2in-2out states with net magnetizations along one of the six cubic $\{001\}$ directions. In Fig. 7(a), the directions of the individual magnetic moments are indicated by the arrows, which on a larger scale average to a vanishing total magnetization. A single spin flip needs an excitation energy of 2.2 K (3.3 K) for $Dy_2Ti_2O_7$ ($Ho_2Ti_2O_7$), see Fig. 3, and creates a pair of neighboring tetrahedra in the 3in-1out and the 1in-3out configurations as indicated by the red and blue circles, respectively, in Fig. 7(b). Now it is straightforward to see that, by applying successive additional spin flips, the positions of the excited tetrahedra may separate from each other without increasing the number of excited tetrahedra. This is a consequence of the degeneracy of the 2in-2out states and, in the example of Fig. 7(c), the marked arrows of the yellow squares just switched between different 2in-2out states. Thus, on this level of simplification, the original dipole excitation fractionalizes into 2 independent monopole excitations without additional energy cost.

Fractionalized excitations are a typical feature of one-dimensional models, e.g., a ferromagneti-

cally ordered chain of Ising spins. There, the lowest excitation corresponds to a single spin flip, which breaks the bonds to the left and right neighbors. Having excited this state once, successive additional spin flips do not further increase the number of broken bonds, but only change the length of a magnetic domain of inverted spins. Therefore, the single spin flip fractionalizes into 2 independent domain walls, which may propagate freely along the chain. Note that this also applies to the β chains of spin ice, when a finite magnetic field is applied along the α chains. Another example is the antiferromagnetic Heisenberg spin-1/2 chain, where the $S = 1$ triplet excitations fractionalize into pairs of $S = 1/2$ (anti-)spinon excitations. Usually, such a fractionalization is suppressed by a finite $3d$ coupling to neighboring chains and, in general, it does not occur in higher-dimensional systems. This is basically related to the fact that the domain walls of strictly $1d$ chains are independent of the domain length, while in higher dimensions the domain-wall size, and thus the number of broken bonds, increases with increasing domain volume. Therefore, the dipolar spin-ice materials represent the very exceptional case where fractional excitations can be realized in a 3-dimensional system.

Another important aspect is the analogy of these fractional excitations to magnetic monopoles. This can be best visualized within the so-called dumbbell model [11]. For its construction, the dipole vectors (black arrows in Fig. 7) are replaced by dumbbells of opposite magnetic monopole charges $\pm q_m$ at the centers of the 2 neighboring tetrahedra. In order to reproduce the original dipole moment $\mu \simeq 10\mu_{\rm B}$, on has to set $q_m \simeq 10\mu_{\rm B}/r_t \simeq 2.3\,\mu_{\rm B}$/Å, where $r_t = \sqrt{3/2}\, r_{nn}$ is the distance between the centers of neighboring tetrahedra and $r_{nn} \simeq 3.54$ Å denotes the nearest neighbor distance of the magnetic Dy or Ho ions. Each tetrahedron is occupied by 4 magnetic monopole charges, which just cancel to zero for the six 2in-2out configurations, the 3in-1out and 1in-3out states carry $+2q_m$ and $-2q_m$, respectively, while 4in (4out) has a total charge of $+4q_m$ ($-4q_m$). By introducing the net magnetic charge $Q = 2q_m$, one can formulate a magnetic Coulomb law:

$$V(r_{\alpha\beta}) = \begin{cases} \frac{\mu_0}{4\pi}\frac{Q_\alpha Q_\beta}{r_{\alpha\beta}} & \alpha \neq \beta \\ \frac{1}{2}\nu_0 Q_\alpha^2 & \alpha = \beta \end{cases} \tag{4}$$

As is shown in [11], Eq. (4) yields a very good approximation of the original dipolar spin-ice model based on Eq. (1). The tetrahedra are labeled by α, β, the first line describes a (magnetic) Coulomb interaction between charges on different sites and the second line is a self energy, where the parameter ν_0 is given by a lengthy combination of J_{ex}, D_{nn}, and r_{nn}; see [11]. Each tetrahedral site may be occupied either with 0, 1, or 2 charges of $\pm Q$, but there are as many positive as negative charges, because they can only be created pairwise by rotating a dumbbell. With the above constraints (and a large-enough value of ν_0), the groundstate of Eq. (4) at zero energy is given by $Q_\alpha = 0$ for all sites, which obviously corresponds to the 2in-2out states given by the ice rule including their sixfold degeneracy. A minimum excitation requires twice the self energy minus the nearest-neighbor attraction. This corresponds to Fig. 7(b), where the red and blue circles correspond to $+Q$ and $-Q$, respectively, and in (c) the distance $r_{\alpha\beta}$ between the monopole charges has increased. Due to the $1/r_{\alpha\beta}$ potential, it is also clear now that the total energy increases with increasing distance, but nevertheless the $\pm Q$ excitations behave as individual magnetic (anti-)monopoles, because they are asymptotically free in the limit of infinite $r_{\alpha\beta}$. In this sense, the situation is equivalent to electric charges $\pm Q_e$ with the electrostatic $1/r$ Coulomb potential. Of course, there are also clear differences and the model (4) has limitations. A rather detailed discussion of these aspects in comparison to other models, numerical simulations via Monte Carlo simulations and their applicability to reproduce the experimental data of $Dy_2Ti_2O_7$ can be found, e.g., in [29].

Another obvious question is, how the above-described magnetic monopole excitations are related to so-called Dirac monopoles [30], whose existence would explain the quantization of the electric charge e and would also remove the asymmetry of Maxwell's equations with respect to electric and magnetic charges. Despite intense search, no such magnetic monopoles could be observed to date [31] and this statement is independent from the existence or absence of monopole excitations in spin ice. The monopoles in spin-ice are no real particles, but emergent quasi-particles that result from excitations of a strongly interacting many-body system. As such, these monopoles only exist inside the magnetic material and correspond to sources and sinks of the magnetic field $\vec{H}$, whereas the searched Dirac monopoles would correspond to sources or sinks of the magnetic induction $\vec{B}$. Further differences concern the so-called Dirac strings that are attached to the magnetic monopoles as is discussed in more detail in [9, 11]. Nevertheless, the behavior of magnetic monopoles in spin ice should resemble that of real electric charges and thus one may search for signatures of a so-called magnetricity, in analogy to electricity. The perhaps most direct evidence for such an analogy would be to observe a magnetic current as a function of an applied field $\vec{B}$. However, it is of course not possible to attach some kind of 'magnetic cables' to the sample, simply because the existence of such a cable would require the existence of magnetic charges.
Bramwell *et al.* [32] suggested to use the analogy between charges in electrolytes and spin-ice monopoles to study magnetricity. This analogy results from the fact that the (anti-)monopole excitations in spin ice always appear in pairs and interact via the $1/r_{\alpha\beta}$ potential, which is similar to the partial dissociation in electrolytes, e.g. $2\,\mathrm{H_2O} \leftrightarrow \mathrm{H_3O^+} + \mathrm{OH^-}$ of water. Applying an electric field favors the separation of the oppositely charged ions and, as a consequence, the dissociation constant increases. This effect is called the second Wien effect, which for weak electrolytes causes characteristic deviations from Ohm's law due to the electric-field dependent charge-carrier density [33]. Transferring this to magnetricity, one would expect an enhanced density of magnetic (anti-)monopoles in finite external fields. However, for spin ice this analogy does not hold completely, because finite magnetic fields lift the groundstate degeneracy and, as is sketched in Fig. 7(d-f), this suppresses the mobility of the individual (anti-)monopoles. To be more specific, with increasing number of separation steps between the monopole and antimonopole the number of Zeeman-excited 2in-2out states increases and introduces a continuously increasing binding potential. In contrast to the $1/r_{\alpha\beta}$ potential, this additional binding potential will prevent a fractionalization of the dipole excitations into individual (anti-)monopoles. Because the Zeeman energy linearly scales with the magnetic field, this problem can be partially circumvented by using very small external fields. Thus, for $Dy_2Ti_2O_7$ the magnetic-field dependence of μSR data was studied for very small transverse fields $B \leq 3$ mT and from this analysis a magnetic monopole charge $Q \simeq 5\,\mu_\mathrm{B}$/Å was reported in [32], which agrees very well with the value $2q_m \simeq 4.6\,\mu_\mathrm{B}$/Å used in Eq. (4). However, severe doubts about this interpretation have been published by 2 other groups [34, 35], which both studied μSR of $Dy_2Ti_2O_7$ and obtained data that differ from those of [32]. Thus, the experimental determination of the magnetic monopole charge in spin ice remains an open issue.

6 Heat transport in spin ice

In this section, the influence of the spin-ice excitations on the heat transport will be discussed. As the spin-ice materials are good insulators, the heat transport is dominated by phonons and the magnetic excitations may influence the total heat transport in two ways. The magnetic ex-

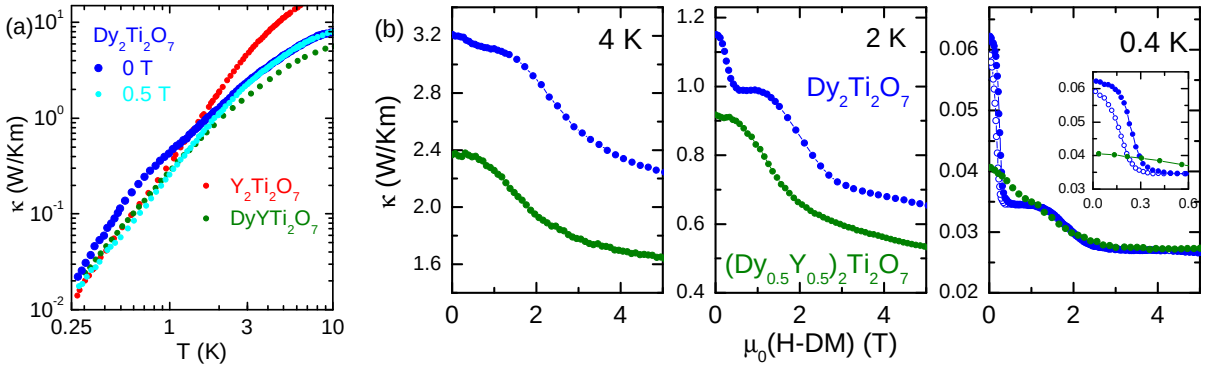

Fig. 8: *(a) Thermal conductivity as a function of temperature for $Y_2Ti_2O_7$ and $DyYTi_2O_7$ in zero field compared to that of $Dy_2Ti_2O_7$ in zero field and $B = 0.5$ T applied along [100]. (b) Comparison of the field-dependent thermal conductivities of $DyYTi_2O_7$ and $Dy_2Ti_2O_7$ for different temperatures. The field scales are corrected with respect to the demagnetization fields DM. The inset is an enlarged view of the region where the $Dy_2Ti_2O_7$ data obtained with increasing (●) and decreasing (○) field are hysteretic. (data from [25, 36]).*

citations may add an additional contribution to the heat transport or they scatter with phonons and therefore suppress the phonon heat transport. In general, both effects are present and as an approximate Ansatz the superposition $\kappa \simeq \kappa_{\rm ph} + \kappa_{\rm mag}$ can be used, where both individual contributions $\kappa_{\rm ph}$ and $\kappa_{\rm mag}$ are reduced from to their hypothetical bare values by phonon-magnon scattering.

From the experimental point of view, the main task is to judge whether there is a sizable magnetic contribution to the overall heat transport. For this, one can compare the temperature and magnetic-field dependences of κ for spin-ice materials with $\kappa(T, H)$ of suitable reference materials, as it is shown in Fig. 8. An ideal non-magnetic reference is $Y_2Ti_2O_7$, which also crystallizes in the pyrochlore structure and the ionic radius of Y^{3+} is located between those of Dy^{3+} and Ho^{3+}. Therefore, it is also possible to study the corresponding dilution series, where Dy^{3+} or Ho^{3+} are partially substituted by Y^{3+} [23, 37]. For larger amounts of non-magnetic Y^{3+} ions, the spin-ice behavior is successively suppressed, because the system changes from being highly frustrated towards highly dilute. This crossover causes a rapid decrease in the low-temperature entropy, which is observed experimentally in $(Dy_{1-x}Y_x)_2Ti_2O_7$ and also in Monte Carlo simulations [23, 38]. Thus, the 50%-diluted material $DyYTi_2O_7$ can serve as a magnetic reference material without spin-ice behavior. Figure 8(a) compares the temperature dependences of $\kappa(T)$ for different materials. In this double-logarithmic representation, the low-temperature data for $Y_2Ti_2O_7$ approach a straight line, that is $\kappa(T) \propto T^{2.4}$, which is close to a T^3 dependence expected for the heat transport of acoustic phonons, and a very similar behavior is found for $\kappa(T)$ of $DyYTi_2O_7$. For $Dy_2Ti_2O_7$, however, the zero-field data show a pronounced shoulder around $T \simeq 1$ K, which is suppressed to a more standard power-law dependence when a small magnetic field of 0.5 T is applied along $[100]$. This already indicates an anomalous $\kappa(T, H)$ of $Dy_2Ti_2O_7$ in the field and temperature range, where the spin-ice physics is dominant, see Fig. 4. A direct comparison of the field dependences $\kappa(H)$ is shown in Fig. 8(b). For $Y_2Ti_2O_7$, κ does not change as a function of field [36], as expected for a non-magnetic insulator. In contrast, $\kappa(H)$ considerably decreases with increasing field for both Dy-based materials and above about 1 T the shape of the $\kappa(H)$ curves is very similar. In contrast, at $T \leq 2$ K and fields below 0.5 T, there is an additional step-like decrease of κ of $Dy_2Ti_2O_7$, which is almost completely absent in

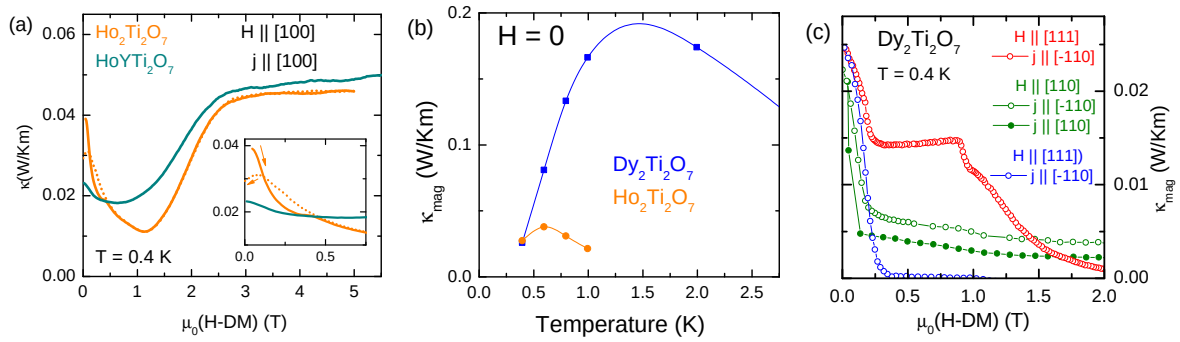

Fig. 9: *(a) Magnetic-field dependent thermal conductivities of $HoYTi_2O_7$ and $Ho_2Ti_2O_7$ for $H\|[110]$. The inset enlarges the low-field range. (b) Zero-field magnetic contribution $\kappa_{\rm mag}$ of the heat transport as a function of temperature for $Dy_2Ti_2O_7$ and $Ho_2Ti_2O_7$. (c) Anisotropy of $\kappa_{\rm mag}$ of $Dy_2Ti_2O_7$ with respect to different magnetic-field directions. For $H\|[110]$, the heat current j is directed either along the α ($j\|H, \bullet$) or the β chains ($j \perp H, \circ$). Field scales in (a) and (c) are corrected with respect to the demagnetization fields DM. (data from [36, 37]).*

κ of $DyYTi_2O_7$. This yields clear evidence that the low-field drop of κ is characteristic for the spin-ice phase. This conclusion is further confirmed by the very similar hysteresis behavior of $\kappa(H)$ and $M(H)$ observed below about 0.5 K. In contrast, the continuous decrease of $\kappa(H)$ at higher fields is not related to the spin-ice phase, it is also present in the highly dilute $DyYTi_2O_7$ and, moreover, it extends to a field range where the magnetization is essentially saturated.
Surprisingly, $\kappa(H)$ of the Ho-based pyrochlore materials has a very different high-field dependence. As is shown in Fig.9(a), κ strongly increases above about 1.5 T and essentially saturates above 3 T. Such a behavior usually indicates that the phononic heat transport at low fields is reduced due to scattering between phonons and magnetic excitations, and this scattering channel is suppressed when the magnetic moments become fully polarized in high fields. However, such a field-dependent scattering of phonons cannot explain, why the heat transport in the Dy-based materials actually decreases at high fields, and it was speculated that this difference is related to magnetostriction effects [37]. With respect to the spin-ice phase, a detailed understanding of the high-field behavior is not absolutely necessary. It is sufficient to realize that for both, the Ho-based and the Dy-based systems, the high-field dependence remains essentially unchanged when the pure spin-ice compounds are dilute with 50 % of non-magnetic Y, whereas the step-like decrease of $\kappa(H)$ at very low field is only present in the respective spin-ice materials.
Because for $H\|[100]$ the step in κ (anti-)correlates with the step-like increase of the magnetization to saturation [25], the step height of κ can be used as a measure of the magnetic contribution $\kappa_{\rm mag}$ of the heat transport in zero field. This has been evaluated at different temperatures and, as shown in Fig. 9(b), the corresponding $\kappa_{\rm mag}(T)$ for $Dy_2Ti_2O_7$ has a broad maximum around 1.5 K, which strongly resembles the temperature dependence of the magnetic specific heat $c_{\rm mag}(T)$, see Fig. 6. For $Ho_2Ti_2O_7$, $\kappa_{\rm mag}(T)$ is of similar shape, but it is reduced in size and its maximum is located around 0.6 K. Finally, Fig. 9(c) compares the anisotropic magnetic-field dependences of $\kappa_{\rm mag}(T = 0.4\,{\rm K})$ for $Dy_2Ti_2O_7$ and reveals an interesting correlation: the maximum $\kappa_{\rm mag}$ is obtained for the sixfold degenerate zero-field groundstate, this is followed by a rather large plateau value of $\kappa_{\rm mag}$ in the threefold degenerate kagome-ice phase for $\mu_0 H \leq 1$ T $\|[111]$, whereas $\kappa_{\rm mag}$ vanishes in the fully magnetized states for $H\|[100]$ and $H\|[111]$, which are non-degenerate. For $H\|[110]$, there is also an initial drop of $\kappa_{\rm mag}$, but only to a finite value, which slowly decreases with further increasing field. Probably, this finite $\kappa_{\rm mag}$

stems from the β chains whose moments are not fixed by the perpendicular magnetic field. This would explain why this finite $\kappa_{\rm mag}$ is larger for a heat current j along the β chains than for j along the α chains. Thus, the anisotropy of $\kappa_{\rm mag}$ essentially reflects the different degeneracies of the field-induced spin-ice groundstates and suggests that $\kappa_{\rm mag}$ is determined by the mobility of the (anti-)monopole excitations.
Unfortunately, theoretical predictions about the expected magnitude of $\kappa_{\rm mag}$ due to monopole excitations in spin ice are difficult. On the one hand, their energy scale is low, while, on the other hand, their mobility due to the fractionalization could be rather high. The fractionalization together with the strong Ising character of the magnetic moments are problematic, because standard descriptions based on wave-like quasiparticle excitations cannot be applied here. This makes reliable estimates of a monopole mean-free path very difficult [25, 39] and it remains an open issue whether the anomalous $\kappa_{\rm mag}$ of $Dy_2Ti_2O_7$ can also quantitatively be explained by (anti-)monopole excitations.

7 Concluding remarks

Intense research over the last 2 decades has led to a very deep understanding of many aspects of the dipolar spin-ice materials $Ho_2Ti_2O_7$ and $Dy_2Ti_2O_7$ and it is generally accepted that they represent the magnetic analogue of ordinary water ice. Nevertheless, the ultimate low-temperature behavior of these spin-ice materials remains an open issue. Concerning the excitations, there is lots of more or less indirect evidence that a description based on essentially unbound magnetic monopole/antimonopole pairs is most appropriate, but again, a direct proof of, e.g., a monopole charge is still a matter of debate. In addition, there are many other open questions. One example, concerning the magnetic heat transport has been described in some detail, but there are many more open issues concerning the dynamics of the magnetic excitations of spin ice, which are not yet understood.

References

[1] M.J. Harris, S.T. Bramwell, D.F. Mcmorrow, T. Zeiske, and K. W. Godfrey. Physical Review Letters **79**, 2554 (1997).

[2] J.D. Bernal and R.H. Fowler. J. Chem. Phys. **1**, 515 (1933).

[3] Linus Pauling. J. Am. Chem. Soc. **57**, 2680 (1935).

[4] S.T. Bramwell and M.J. Gingras. Science **294**, 1495 (2001).

[5] D.J.P. Morris, D.A. Tennant, S.A. Grigera, B. Klemke, C. Castelnovo, R. Moessner, C. Czternasty, M. Meissner, K.C. Rule, J.U. Hoffmann, K. Kiefer, S. Gerischer, D. Slobinsky, and R.S. Perry. Science **326**, 411 (2009).

[6] Leon Balents. Nature **464**, 199 (2010).

[7] H. Bethe. Zeitschrift f. Physik **71**, 205 (1931).

[8] Jason S. Gardner and John E. Greedan. Rev. Mod. Phys. **82**, 53 (2010).

[9] A.A. Zvyagin. Low Temperature Physics **39**, 901 (2013).

[10] I.A. Ryzhkin. J. Exp. Theor. Phys. **101**, 481 (2005).

[11] C. Castelnovo, R. Moessner, and S.L Sondhi. Nature **451**, 42 (2008).

[12] Jeffrey G. Rau and Michel J.P. Gingras. Physical Review B **92** (2015).

[13] SungBin Lee, Shigeki Onoda, and Leon Balents. Physical Review B **86**, 104412 (2012).

[14] M.J.P. Gingras and P.A. McClarty. Rep. Prog. Phys. **77**, 056501 (2014).

[15] Roger G. Melko and Michel J.P. Gingras. J. Phys. Cond. Matt. **16**, R1277 (2004).

[16] S.T. Bramwell, M.J. Harris, B.C. den Hertog, M.J.P. Gingras, J.S. Gardner, D.F. Mcmorrow, A.R. Wildes, A.L. Cornelius, J.D.M. Champion, R.G. Melko, and T. Fennell. Physical Review Letters **87**, 047205 (2001).

[17] B.C. den Hertog and M.J.P. Gingras. Physical Review Letters **84**, 3430 (2000).

[18] A.P. Ramirez, A. Hayashi, R.J. Cava, R. Siddharthan, and B.S. Shastry. Nature **399**, 333 (1999).

[19] T. Bartels-Rausch, V. Bergeron, J.H.E. Cartwright, R. Escribano, J.L. Finney, H. Grothe, P.J. Gutiérrez, J. Haapala, W.F. Kuhs, J.B.C. Pettersson, S.D. Price, C.I. Sainz-Díaz, D.J. Stokes, G. Strazzulla, E.S. Thomson, H. Trinks, and N. Uras-Aytemiz. Rev. Mod. Phys. **84**, 885 (2012).

[20] W. F. Giauque and Muriel F. Ashley. Physical Review **43**, 81 (1933).

[21] W. F. Giauque and J W Stout. J. Am. Chem. Soc. **58**, 1144 (1936).

[22] D. Pomaranski, L.R. Yaraskavitch, S. Meng, K.A. Ross, H.M.L. Noad, H.A. Dabkowska, B.D. Gaulin, and J.B. Kycia. Nature Physics **9**, 353 (2013).

[23] S. Scharffe, O. Breunig, V. Cho, P. Laschitzky, M. Valldor, J.F. Welter, and T. Lorenz. Physical Review B **92**, 180405 (2015).

[24] B. Klemke, M. Meissner, P. Strehlow, K. Kiefer, S.A. Grigera, and D.A. Tennant. J. Low Temp. Phys. **163**, 345 (2011).

[25] G. Kolland, O. Breunig, M. Valldor, M. Hiertz, J. Frielingsdorf, and T. Lorenz. Physical Review B **86**, 060402(R) (2012).

[26] T. Fennell, M. Kenzelmann, B. Roessli, H. Mutka, J. Ollivier, M. Ruminy, U. Stuhr, O. Zaharko, L. Bovo, A. Cervellino, M.K. Haas, and R.J. Cava. Physical Review Letters **112**, 017203 (2014).

[27] P.A. McClarty, O. Sikora, R. Moessner, K. Penc, F. Pollmann, and N. Shannon. Physical Review B **92**, 094418 (2015).

[28] Arnab Sen and R. Moessner. Physical Review Letters **114**, 247207 (2015).

[29] C. Castelnovo, R. Moessner, and S. L. Sondhi. Physical Review B **84**, 144435 (2011).

[30] P.A.M. Dirac. Physical Review **74**, 817 (1948).

[31] Kimball A. Milton. Rep. Prog. Phys. **69**, 1637 (2006).

[32] S.T. Bramwell, S.R. Giblin, S. Calder, R. Aldus, D. Prabhakaran, and T. Fennell. Nature **461**, 956 (2009).

[33] Lars Onsager. J. Chem. Phys. **2**, 599 (1934).

[34] S. Dunsiger, A. Aczel, C. Arguello, H. Dabkowska, A. Dabkowski, M.H. Du, T. Goko, B. Javanparast, T. Lin, F. Ning, H. Noad, D. Singh, T. Williams, Y. Uemura, M. Gingras, and G. Luke. Physical Review Letters **107**, 207207 (2011).

[35] Stephen J. Blundell. Physical Review Letters **108**, 147601 (2012).

[36] G. Kolland, M. Valldor, M. Hiertz, J. Frielingsdorf, and T. Lorenz. Physical Review B **88**, 054406 (2013).

[37] S. Scharffe, G. Kolland, M. Hiertz, M. Valldor, and T. Lorenz. JPS Conf. Proc. **3**, 014030 (2014).

[38] T. Lin, X. Ke, M. Thesberg, P. Schiffer, R.G. Melko, and M.J.P. Gingras. Physical Review B **90**, 214433 (2014).

[39] S.J. Li, Z.Y. Zhao, C. Fan, B. Tong, F.B. Zhang, J. Shi, J.C. Wu, X.G. Liu, H.D. Zhou, X. Zhao, and X.F. Sun. Physical Review B **92**, 094408 (2015).